15TH IEA HEAT PUMP CONFERENCE
MAY 26–29, 2026 | HOFBURG
VIENNA 2026
DECARBONISATION THROUGH INNOVATION

Development of a HTHP design tool for an industrial waste heat recovery system integrated with a two-phase variable geometry ejector and IHX using natural refrigerants

Rui Silva[a,b], Szabolcs Varga[a,b], João Soares[a,b], Karla Jacinto[a,b], Armando Oliveira[a,b]

[a]*INEGI - Institute of Science and Innovation in Mechanical and Industrial Engineering*, Rua Dr Roberto Frias, Porto 4200–465, Portugal
[b]*FEUP - Faculty of Engineering, University of Porto*, Rua Dr Roberto Frias, Porto 4200–465, Portugal

Abstract

The accelerated use of thermal energy by industrial sector is accompanied by an increase in waste heat rejection. High-temperature heat pumps (HTHPs) could significantly improve the overall energy efficiency and contribute to energy circularity of industrial processes by enabling waste heat recovery back to process temperatures through temperature upgrade. However, the general requirement for high temperatures in the industrial sectors constitute a technological challenge. The present work focuses on the design and performance assessment of an HTHP in an innovative configuration integrating a two-phase variable geometry ejector (VGE) for expansion work recovery and an internal heat exchanger. A numerical design tool was developed and applied for studying the use of five different environmentally friendly working fluids. VGE features considered allow the active adjustment of the ejector area ratio and the hypothetical throat section using a spindle and a changeable primary nozzle exit position. The model is based on the application of mass and energy conservation principles for the individual system components and for VGE cross-sections, applying real gas thermodynamic properties. The simulations were conducted, in the EES software, for a small-scale unit with a minimal heat output of 20kW at constant temperature of 130ºC and with a gross temperature lift range from 30ºC to 60ºC. The results showed that R601 performed the best for the operating range considered. For R601 and a temperature lift of 60ºC, it was found that VGE integration can lead to electrical consumption by 15% (COP=3.1) lower than without the ejector. Similarly, for the same heat output, compressor flow rate decreased by 23% which also contributes to a reduced sensitivity of the cycle to variable operating conditions. Based on the results, it is concluded that the integration of a VGE into the HTHP systems is highly beneficial both in terms of performance and operation stability.

Selection and/or peer-review under the responsibility of the organizers of the 15th IEA Heat Pump Conference 2026.

Keywords: High-temperature heat pumps (HTHP); Two-phase variable geometry ejector (VGE); Industrial waste heat upgrade; Fluid parametric study; Numerical design tool; System performance..

1. Introduction

Nations worldwide acknowledge the necessity of moving toward a low-carbon, climate-resilient economy and must substantially intensify efforts to meet internationally agreed greenhouse gases reduction targets [1]. From a theoretical standpoint, high-temperature heat pumps (HTHP) that recover waste heat and are powered by renewable electricity offer significant potential to disruptively decarbonise industry's heat requirements [2]. The industrial sector is the dominant consumer of heat, accounting for close to 20% of worldwide energy consumption [3]. EU industrial heat needs at 80ºC-150ºC are around 75 TWh/year, while recoverable low-temperature waste heat is on the order of 100 TWh/year, indicating substantial scope for HTHP integration [4].

The findings reported in [5], present the distribution of cumulative waste heat and process heat across different temperature levels for a selection of European industrial sectors. Upgrading waste heat under 100ºC to process temperatures exceeding 130ºC would make heat-pump technology advantageous across all assessed industrial sectors [5], improving systems energy efficiency and exergetic performance as mentioned by [6,7].

Different HTHP system configurations and their performance were published by [6–8], for different working fluids. The optimal working fluid has not yet been found, but it should be thermodynamically adequate to the pretended operating conditions, environmentally friendly (zero/negligible GWP and ODP values), future-proof, efficient and commercially available [4,6]. The mostly tested alternatives for HTTPs are R1234ze(Z), R1366mzz(Z), R1233zd(E), HCFO-1224yd(Z), R600 and R601 [6,9]. Fluid selection consists in a compromise between obtained system performance (COP) and volumetric heating capacity (VHC), usually resulting in a multi-objective approach [7].

With increasing heat upgrade temperatures, technological barriers occur regarding system design hence the engineering experience gathered with conventional HPs cycles does not necessarily apply to high-temperature systems [6]. Additionally, as HTHP's temperature lift increases, so does the required compression ratio (CR) and the corresponding expansion losses. This leads to a simultaneous compressor efficiency and cycle performance reduction. One promising HTHP cycle improvement is the use of ejectors, considering their simplicity, absence of moving parts, robust structure and low-cost (initial and operational) [10], and the ability to partially recover expansion work and reduce the compression ratio [11]. An assessment for advanced HTHP cycles shows that the ejector and internal heat exchanger (IHX) simultaneous integration conducted to the best balance between the COP and VHC [7].

Bai et al. [11] showed that ejectors use could have a beneficial impact on system performance (14% COP increase), yet, it could decrease for others. These results were justified by the strong dependence of the optimal ejector geometry for different operating conditions [12]. In these advanced cycles, the ejector is a critical component for energy savings, and the performance is significantly affected by the variable operating conditions (such as heat demand, waste heat availability and source temperatures) encountered in many industrial sectors [13]. Ideally, neither HTHP nor ejector performance should be significantly affected by off-design operations, however experimental data showed that the cycle COP decreased (>25%) when the heat pump temperature lift increased from 50ºC to 60ºC for constant sink temperature of 140ºC [6]. Thus, by using a conventional ejector, the benefits could turn into a negative impact under when the system operates under variable conditions. In order to overcome this problem in ejector assisted heat pump systems a relatively complex multi-ejector solution was proposed by [14]. Alternatively, a simpler and more cost effective solution based referred to as a variable geometry ejector (VGE) could be designed [15–19]. Given the potential advantages, the presented work addresses the performance analysis of a HTHP system integrating a VGE under changing heat source temperature conditions. The analysis was performed using a numerical approach that included the development two specific design tool, one for the heat pump cycle and another one for the VGE design. The results were compared to a system applying a internal heat exchanger only, for reference.

2. HTHP and VGE Theoretical Models

2.1. Considered system configurations and cycle models

A schematic representation of the modelled heat pump system is shown in Figure 1. It is composed by an evaporator, mechanical compressor (MC), condenser, an IHX, the VGE, separator (SEP), expansion (ExV) and regulation valves (BV). Depending on the positioning of the regulation valves, the system can operate in 2 different configurations: heat pump with internal heat exchanger and a heat pump with IHX and VGE. The regulation valves are either fully closed or fully open. The representative thermodynamic states of the working fluids are also identified by numbers in Figure 1.

Figure 2 shows the modelled thermodynamic processes of the working fluid state (1-9) on a p-h diagram in the VGE cycle. Several model parameters were considered for the simulations. These parameters are summarised in Table 1. The mathematical model was developed by applying the mass and energy conservation laws for each cycle component. These equations are relatively well known, for their specific forms the reader is referred to [7].

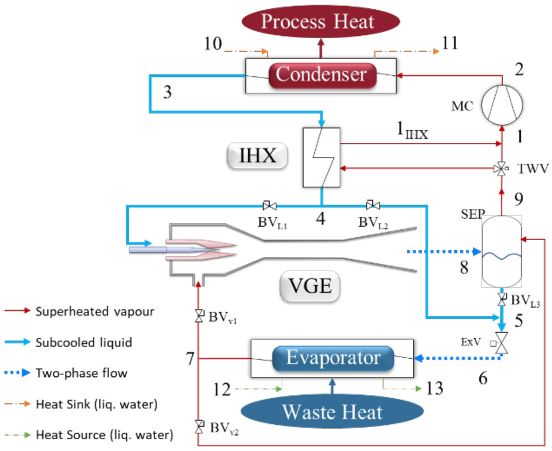

Figure 1. Schematic HTHP system diagram with main components and their hydraulic connections.

The HTHP thermodynamic numerical model was developed with the following assumptions:

- Steady state operation;
- The working fluid with real fluid properties obtained from EES's (Fchart, USA) built-in library;
- Homogeneous equilibrium between phases during two-phase processes;
- Negligible pressure losses during fluid transport;
- Isenthalpic expansion in valves;
- Subcooled water as heat source and heat sink working fluid;
- Nominal heating capacity of 20 kW;
- Separator efficiency of 100%.

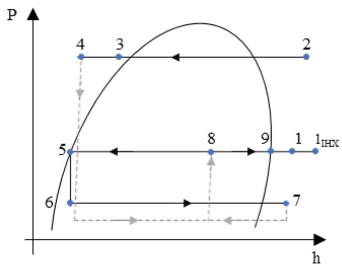

Figure 2. Theoretical P-h state diagram for the VGE cycle

Table 1. HTHP-VGE Model parameters with their values applied during the simulations.

Parameter	Assumed Value	Units
Heat Source Inlet Temperature (T_{src_in})	[70, 100]	ºC
Heat Sink outlet Temperature (T_{sk_out})	130	ºC
Evaporator Glide Temperature ($T_{e\ glide}$)	10	K
Condenser Glide Temperature ($T_{c\ glide}$)	10	K
Evaporator Pinch Point Temperature ($T_{e\ pp}$)	2	K
Condenser Pinch Point Temperature ($T_{c\ pp}$)	5	K
Evaporator Superheat degree (SH_e)	10	K
Condenser Superheat degree (SH_c)	2	K
Condenser Subcooling degree (SC_c)	10	K
Compressor's Isentropic Efficiency ($\eta_{is_{MC}}$)	0.8	-
Compressor's Volumetric Efficiency ($\eta_{v_{MC}}$)	0.85	-
Compressor's Electromechanical Efficiency ($\eta_{em_{MC}}$)	0.85	-
IHX efficiency (ε_{IHX})	0.7	-

The heat transfer in the heat exchanger was modelled using the heat exchanger efficiency formula. As an example, the efficiency for the internal heat exchanger (ε_{IHX}) can be defined as:

$$\varepsilon_{IHX} = \frac{h_{1_{IHX}} - h_9}{h_{max_{IHX}} - h_9} \tag{1}$$

In Eq.1, h_9 represents specific enthalpy at separator outlet assuming saturated vapor (9), while $h_{1_{IHX}}$ is the specific enthalpy at IHX vapor outlet (1_{IHX}), and $h_{max_{IHX}}$ is the maximum achievable specific enthalpy at 1_{IHX} (with $T_{1_{IHX}} = T_3$). The compressor electric power consumption and the volumetric flow rate at the compressor inlet (1) were estimated using:

$$\dot{P}_{mc} = \frac{(h_2 - h_1) \cdot \dot{m}_c}{\eta_{em_{mc}}}, \tag{2}$$

$$\dot{V}_{mc} = \frac{\dot{m}_c/\rho_1}{\eta_{v_{mc}}}, \tag{3}$$

where $\eta_{em_{mc}}$ and $\eta_{v_{mc}}$ are compressor electromechanical and volumetric efficiency constants (see Table 1). The heat pump coefficient of performance (COP) was determined as the ratio of the HTHP heating capacity ($\dot{Q}_{cond}$) and $\dot{P}_{mc}$, thus:

$$COP = \frac{\dot{Q}_{cond}}{\dot{P}_{mc}}. \tag{4}$$

When validated against numerical data [7], the developed model predicted a COP value 9% lower for R601.

2.2. VGE Model

A cross-section view of the modelled ejector is shown in Figure 3 with its characteristic dimensions. The ejector is composed by a motive (primary) nozzle, a suction (secondary) chamber, suction (secondary) nozzle, constant area section and diffuser. For detailed description of ejector operation, the reader is referred to [20–22]. The flow geometry inside the ejector was considered to be variable, by independently changing two relevant geometrical factors inside the device, namely the ejector area ratio and the nozzle exit position (NXP). The area ratio is defined as the ratio between the constant area and the primary nozzle throat sections. This can be adjusted by changing the nozzle throat area using a variable diameter spindle with axial movement. NXP is defined as the distance of the nozzle exit plane from the constant area section inlet. The spindle position (SP) was considered zero when the spindle completely blocked the primary flow passage through the nozzle throat, with a positive direction upstream (see Figure 3). For more details of the VGE concept the reader is referred to [15,23–25].

The VGE design model was developed with the following assumptions:

- Steady state one-dimensional flow;
- Working fluid with real fluid properties;
- Homogeneous Equilibrium Model (HEM) for the two-phase ejector flow;
- Adiabatic ejector wall;
- Predefined mass flow rate and thermodynamic state at ejector inlets (inputs from HTHP model);
- Isentropic efficiency constants to account for irreversibilities;
- Chocked motive flow in primary nozzle throat (M_a=1);
- Static pressure at primary nozzle outlet section (no) 5% lower than at secondary stream (so);
- Hypothetical throat (secondary stream choking) inside the constant area section;
- Primary and secondary streams have the same pressure at hypothetical throat
- Constant pressure mixing;
- Normal shock of zero thickness at the end of the constant area section;
- Subsonic flow in the diffuser section.

The developed model is based on applying the energy and mass conservation equations between a set of physical and hypothetical cross sections within the ejector including, motive nozzle inlet (ni), throat (nt) and outlet (no), as well as suction chamber inlet (si) and outlet (sc), the secondary stream at primary nozzle outlet (so), hypothetical throat (py , sy), mixing (mo), shock (as), and diffuser outlet (d). The location of these sections is indicated in Figure 3. A detailed description of the mathematical formulas can be found in [26–29]. Here, only the differences in the modelling approach are pointed out.

The constant-pressure mixing approach assumes the existence of a hypothetical throat within the constant-area section, as also described in [29]. The hypothetical throat is the location where the secondary stream reached Ma_{sy}=1. By writing the energy conservation law for the secondary steam between the nozzle exit plane, one can obtain the following relationship:

$$h_{so} + 0.5 \cdot v_{so}^2 = h_{sy} + 0.5 \cdot v_{sy}^2 \, . \tag{5}$$

In the equation above h_{so} and v_{so} represent the specific enthalpy and velocity for the entrained flow at primary nozzle exit plane (so). From the isentropic efficiency definition, the secondary stream specific enthalpy at sy section (h_{sy}) can obtained from:

$$h_{sy} = h_{so} - \eta_{is_v} \cdot \left(h_{so} - h_{sy_{is}}\right) , \tag{6}$$

where η_{is_v} represents the isentropic efficiency constant (see Table 2) and $h_{sy_{is}}$ is the fluid specific enthalpy that is obtained by assuming an isentropic expansion. Coupling Eq.s 5 and 6 with the condition Ma_{sy}=1, the secondary stream specific enthalpy (h_{sy}) and velocity (v_{sy}) at ejector hypothetical throat (sy section) can be calculated. Similarly, the energy conservation law can be applied between the motive nozzle outlet (no) and the hypothetical throat (py) sections, using the isentropic efficiency definition and constant pressure mixing assumption (P_{sy}=P_{py}=P_y), from which the thermodynamic properties can be obtained for both streams in the hypothetical throat.

As already stated, mixing process starts at the hypothetical throat and concludes in the mixing section. A mixing efficiency (φ_{mix}) was considered to account for the irreversibilities during the momentum transfer from the primary and secondary streams between the primary nozzle exit plane (no and so sections) and the mixing section (mo) according to:

$$\left(P_{no} \cdot A_{no} + v_{no} \cdot \dot{m}_p\right) + \left(P_{so} \cdot A_{so} + v_{so} \cdot \dot{m}_s\right) = \frac{P_{mo} \cdot A_{mo} + v_{mo} \cdot \left(\dot{m}_p + \dot{m}_s\right)}{\varphi_{mix}}. \tag{7}$$

In Eq.7, the left-hand side terms represent the total momentum at primary nozzle exit, with A_{no} and A_{so} being the available cross section for primary and secondary streams. NXP was adjusted in order to maintain a specific area relation between A_{no} and A_{so}, thereby satisfying the assumption that P_{no} was 5% lower than P_{so}. The primary and secondary mass flow rates are represented by $\dot{m}_p$ and $\dot{m}_s$, respectively. On the right-hand side of Eq.7, is the total fluid momentum corrected by the mixing-induced dissipative effects that are quantified by the mixing efficiency. In existing literature models, φ_{mix} is typically an input value (e.g. [28]), here it was calculated from the ejector outlet properties, which were calculated from the adiabatic ejector assumption. Given that the kinetic energy at the ejector boundaries are negligible, fluid enthalpy at diffuser outlet (d) can be directly obtained from the inlet enthalpies as:

$$\dot{m}_p \cdot h_{ni} + \dot{m}_s \cdot h_{si} = \left(\dot{m}_p + \dot{m}_s\right) \cdot h_d \tag{8}$$

This approach permitted the calculation of the velocity of the mixed fluid (v_{mo}) and thus φ_{mix} from Eq.8.

In order to establish the fluid properties in the nozzle throat and hypothetical throat sections with the double chocked flow assumption, a suitable speed of sound model was needed for the two-phase flow. There are several modes available in the literature including the ones in [28,30–33]. In this work, the model proposed in [33] was selected, since this model was found to perform well for ejector flow simulations [32].

Ejector geometry is typically characterised by the diameter of the different cross sections indicated in Figure 3. Ejector length and convergent/divergent angles are usually defined on recommendations or by more detailed simulations of the flow field, such as using CFD [23]. By applying the conservation laws to the different parts of the ejector with suitable boundary conditions, the resulting set of closed-from non-linear equations can be solved iteratively. Besides working fluid type, typical inputs to the ejector design model were boundary conditions including the primary mass low rate, working fluid enthalpies and pressures. Typical model results included ejector diameters, SP, NXP and compression ratio.

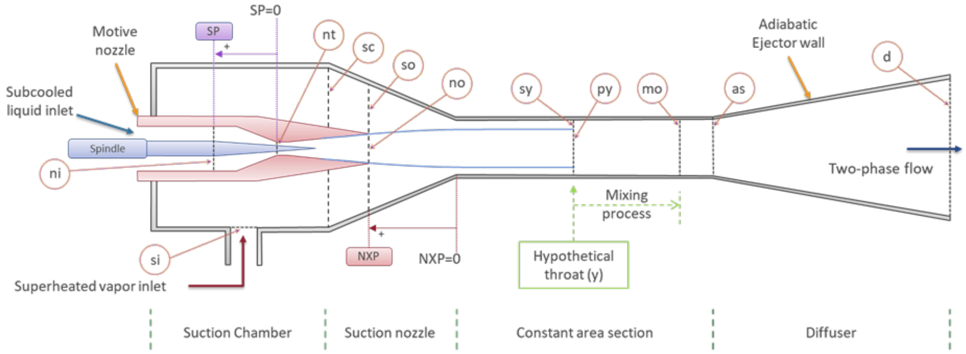

Figure 3. Two-phase VGE cross-section view indicating the reference position for the spindle (SP) and nozzle exit plane (NXP).

Table 2. Applied isentropic efficiencies in the VGE design model.

Isentropic Efficiencies	Assumed Value	Units
Vapour phase flow (η_{is_v})	0.99	-
Two-phase flow ($\eta_{is_{2f}}$)	0.98	-
Two-phase flow inside ejector diffuser (η_{is_d})	0.7	-

3. Solution Strategy

Both the HTHP cycle model and the variable geometry ejector design model were implemented in the EES software (FChart,USA). From the numerical point of view, it was found beneficial to separate the VGE design model from the HTHP-VGE cycle model. As it was already stated, the heat pump model is capable to simulate the heat pump performance in two different configurations (IHX and VGE) for a set of operating conditions. Within this work, the performance of both heat pump configurations was studied for a nominal heating capacity of 20 kW and for a range of heat source temperatures, varying from 70ºC to 100ºC corresponding a temperature lift between 60ºC and 30ºC, respectively. When the IHX configuration was selected, cycle performance indicators were calculated from the heat pump model only. In order to make a direct comparison to the VGE configuration, the heating capacity of the IHX heat pump was set to the same value as in the equivalent VGE configuration, thus it was an input.

In VGE configuration mode, the heat pump model required the ejector compression ratio (CR) and secondary fluid mass flow rate (evaporator mass flow rate) as inputs. These two variables however, depend on both the ejector geometry and ejector inlet boundary conditions. Therefore, to avoid numerical issues, the heat pump model and the ejector design model were solved iteratively until both models converged for the same ejector compression ratio values.

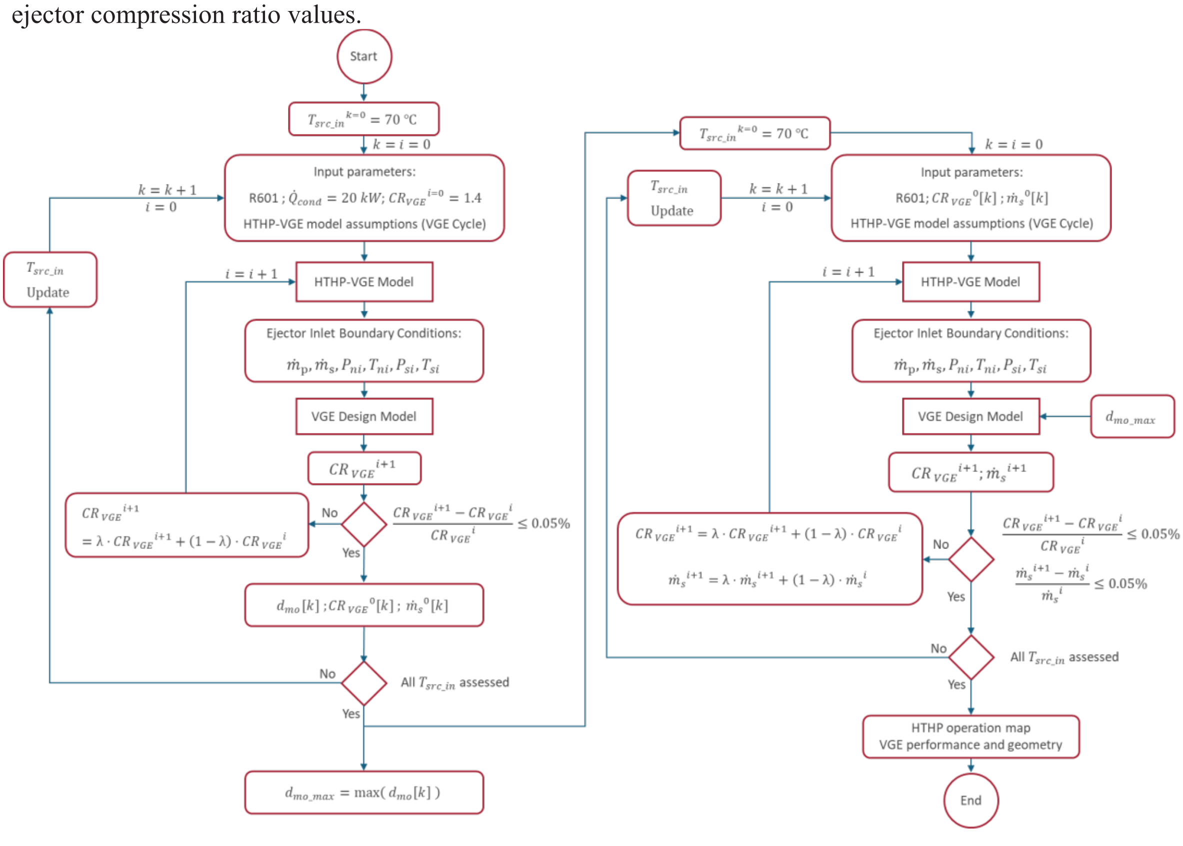

Figure 4. Simplified graphical flow chart of the developed iterative scheme.

The actual iterative process is demonstrated in Figure 4. It started by running the VGE cycle model (HTHP-VGE) using inputs such as the target heat pump capacity and working fluid type. It also required an initial guess for the ejector compression ratio ($CR_{VGE}{}^{i=0}$) and the heat source temperature ($T_{src_{in}}{}^{0}$), usually the lowest one within the considered range (70 – 100ºC). The model then calculated the boundary conditions for the ejector inlet, including mass flow rates and fluid thermodynamic properties. With these boundary conditions the ejector design model was run to determine the required ejector geometry and the actual compression ratio. This CR (${CR_{VGE}}^{i+1}$) was compared to the values in the previous iteration for convergence check. When the convergence criteria were not met, a new value was assumed for the compression ration using a relaxation factor (λ) of 0.5 and the process was repeated. In case of convergence, the heat source inlet temperature was updated to the next value and the iterative process was repeated.

After concluding these simulations, a set of ejector flow and geometry data were available for the 20 kW heating capacity case. The reference (design) geometry was set considering the case that resulted in the largest constant area section (d_{mo_max}) from the parametric analysis. Then the whole process above was again repeated considering the reference ejector geometry as input and by setting the capacity of the heat pump as output. In this case, the iterative process between the heat pump cycle model (HTHP-VGE) and the ejector design model was continued until convergence was obtained for both the ejector compression ratio and the secondary mass flow rate values. As a result, the whole operation map for the high temperature heat pump cycle, integrating the variably geometry ejector, could be constructed for the selected working fluid and the considered heat source temperature range.

4. HTHP performance analysis results

4.1. Fluid Selection

One of the objectives of the present work was to find a suitable low-GWP working fluid for the HTHP-VGE system that leads to high performance [6,8]. Additionally, working fluids only with a critical temperature above 150ºC were considered as candidates in order to keep the entire cycle sub-critical. From these conditions the following refrigerants were selected for the analysis: Cyclopentane, iso-pentane (R601a), n-pentane (R601), butane (R600) and water (R718). A set of performance indicators were determined for the for $\dot{Q}_{cond} = 20$ kW and $CR_{VGE} = 1.4$ (VGE cycle only).The mean values for these performance indicators are shown in Figure 5 for the entire range of heat source temperatures. It can be seen from the figure that water requires the highest compression ratio and flow rate to deliver the nominal heating capacity. Additionally, without suitable cooling mechanism, compressor outlet temperature would be too high (> 400ºC). The estimated COP values (3.8/4.6) were among the lowest recorded within the set of cases considered. The simulations indicated that COP was the lowest for R600 (3.5/4.8), however using Butane presents the lowest compressor compression ratio and volumetric flow rate at the compressor inlet, which can be considered as a positive aspect regarding the mechanical compressor selection. Cyclopentane performed the best in terms of COP (4.2/5.4), however it requires the highest compressor compression ratio, flow rate and leads to the highest $T_{com,out}$, when compared to R601a and R600. Therefore, considering the overall performance of the tested fluids, R601 was selected for the detailed performance analysis of the modelled HTHP system.

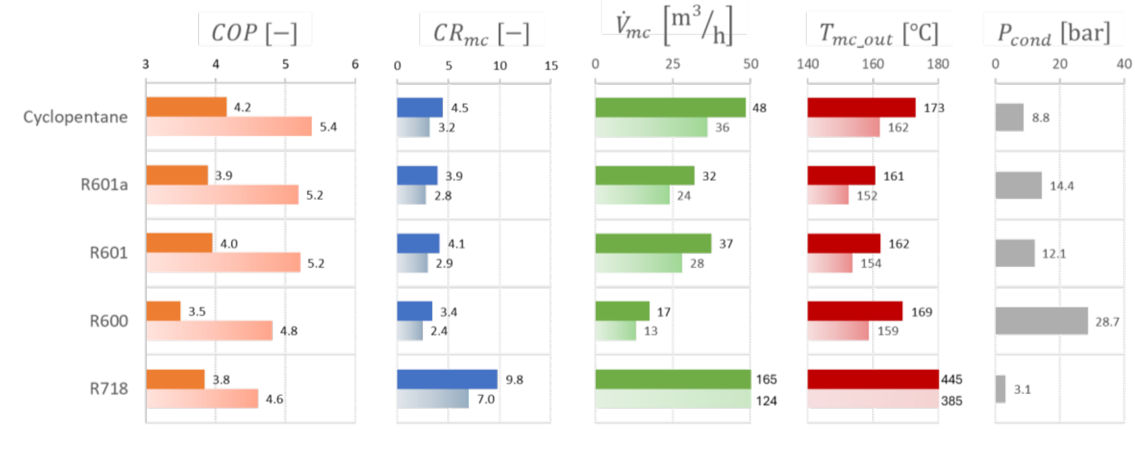

Figure 5. Averaged performance indicators for different working fluids for both IHX (solid colours) and VGE (gradient colours) HTHP cycles.

4.2. HTHP performance analysis for R601

Table 3 summarizes the high temperature heat pump performance maps obtained for both the IHX and VGE configurations. The ejector geometry was obtained by the iterative procedure described in Section 3. The cycle with an internal heat exchanger was assessed for the same heating capacity (but without the ejector). Looking at the data it is clear that the heat pump cycle with the integration of a VGE considerably outperformed the system with an internal heat exchanger only for all indicators. The results for the volumetric flow rate at the compressor inlet are visualised in Figure 6a). It can be observed that the compressor flow rate reduced significantly for the VGE cycle by an average of -16%. Smaller volumetric flow rate reduces mechanical compressor size and thus cost. Another advantage of the VGE cycle is that under variable heat source temperatures, the variability $\dot{V}_{mc}$ is much smaller for the VGE cycle (-17% vs -4%). This reduces the sensitivity of the heat pump performance on compressor speed control and thus assures a more stable operation. Additionally, by applying an ejector, the required compression ratio from the mechanical compressor reduces, especially for lower heat source temperatures. This is visualised in Figure 6b). For lower compression ratio (approximately -17% on average), the mechanical stress on the compressor can be reduced which indirectly affects associated costs.

Table 3. Heat pump performance results for the IHX and VGE cycles for different heat source temperatures.

Operating cond.		IHX cycle						VGE cycle						Performance improvement			
$T_{src_{in}}$	$\dot{Q}_{cond}$	COP	$\dot{Q}_e$	$\dot{Q}_{IHX}$	$\dot{P}_{mc}$	$\dot{V}_{mc}$	CR_{mc}	COP	$\dot{Q}_e$	$\dot{Q}_{IHX}$	$\dot{P}_{mc}$	$\dot{V}_{mc}$	CR_{mc}	ϵ_{COP}	$\epsilon_{\dot{P}_{mc}}$	$\epsilon_{\dot{V}_{mc}}$	$\epsilon_{CR_{mc}}$
ºC	kW	-	kW	kW	kW	m^3/h	-	-	kW	kW	kW	m^3/h	-		%		
70	20.1	2.64	13.7	1.8	7.62	62.0	5.97	3.1	14.6	3.1	6.50	48.0	4.59	17%	-15%	-23%	-23%
75	22.4	2.87	15.8	1.9	7.81	60.2	5.18	3.35	16.7	3.3	6.70	47.8	4.10	17%	-14%	-21%	-21%
80	24.9	3.13	18.1	1.9	7.94	58.3	4.51	3.63	19.1	3.5	6.85	47.6	3.67	16%	-14%	-18%	-19%
85	27.5	3.44	20.7	1.9	8.00	56.6	3.95	3.96	21.6	3.7	6.94	47.3	3.30	15%	-13%	-16%	-16%
90	30.3	3.8	23.5	1.8	7.98	54.8	3.47	4.35	24.4	3.9	6.97	46.9	2.97	14%	-13%	-14%	-14%
95	33.3	4.23	26.6	1.7	7.87	53.1	3.06	4.81	27.4	4.0	6.93	46.5	2.68	14%	-12%	-12%	-12%
100	36.5	4.76	30.0	1.5	7.67	51.5	2.71	5.36	30.7	4.1	6.81	46.0	2.43	13%	-11%	-11%	-10%

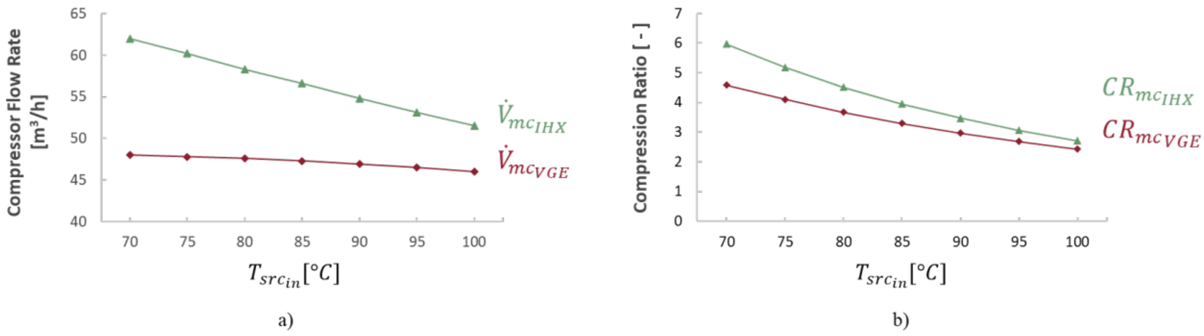

Figure 6. The influence of the heat source temperature on: a) volumetric flow rate at the compressor inlet ($\dot{V}_{mc}$) and b) mechanical ejector compression (CR_{mc}) ratios for both heat pump configurations.

The estimated compressor electric power consumption ($\dot{P}_{mc}$) is visualised in Figure 7a) (see also Table 3). It can be seen that the IHX cycle requires about 7.6~8.0 kW of electricity, depending on the heat source temperature. The maximum electricity consumption was obtained for a heat source temperature of 85ºC, which can be explained by the working fluid properties. When the results are compared to the VGE configuration, one may note that the electric consumption was considerably lower (-13% in average). This is primarily due to the lower required compression ratios for this configuration. It is noted that the reduced flow rate at the compressor inlet would also contribute to an additional reduction of the compressor electricity consumption, however, because of the compressor efficiency constant considered in this work did not depend on the volumetric flow rate, here this effect was not reflected in the results. The reduced electricity consumption and the condition that both studied configurations produced the same amount of heat output is reflected in the calculated COP. These results are depicted in Figure 7b). As expected, COP increased with the heat source temperature for both systems following a non-linear trend. The calculated COP ranged from about 2.6 to 4.8 in case of the IHX cycle, while from about 3.1 to 5.4 when a variable geometry ejector is integrated into system for the tested heat source temperatures. The highest performance improvement was obtained for the design conditions ($T_{src_{in}}$= 70ºC), about 16%, while the lowest for $T_{src_{in}}$=100ºC (~13%).

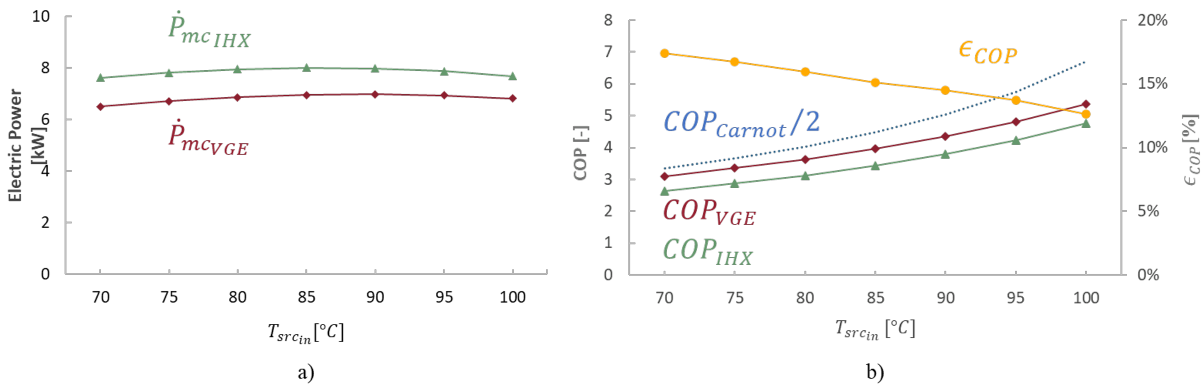

Figure 7. a) Electric power consumption ($\dot{P}_{mc}$) as functions of $T_{src_{in}}$ for both cycle configurations; b) Cycle COP and its relative variation as functions of $T_{src_{in}}$.

It can be concluded from the data presented in Table 3 that the HTHP cycle performance benefits from the integration of a variable geometry ejector into the system. The different cross sections/diameters of the ejector (see Figure 3) were optimised for the design conditions. The variable geometry features, namely the spindle position (SP) and the nozzle exit position (NXP) were determined for each heat source temperature level in order to obtain the highest system performance (highest admissible compression ratio). The results are summarised in Table 4 and the characteristic ejector dimensions are presented in Table 5. Looking at Table 4, one may note that the primary inlet pressure (P_{ni}) remained constant for all cases, because of the constant condensation pressure. The secondary inlet pressure increased with the heat source temperature, because of the increasing evaporation temperature. As a consequence, the achievable entrainment ratio (ER) increased (from 0.56 to 0.67) in agreement with the well-known ejector theory. With increasing heat pump capacity, the primary mass flow rate (equivalent to the condenser mass flow rate of the heat pump) increased. This increase is assured by an increase of the nozzle throat section (choked flow) by moving the spindle to a more open position. Optimal SP increased from 5.3 mm to 16.9 mm, for $T_{src_{in}}$of 70ºC and 100ºC, respectively. With increasing primary mass flow rate, the total energy contained in the primary fluid increased. Simultaneously, the secondary inlet pressure increased with the heat source temperature. Therefore, the results indicated that the optimal NXP reduced with the heat source temperature from about 14 mm to 6 mm. A total spindle travel (~ 11 mm) and NXP adjustment (~ 8 mm) is expected to allow the optimisation of the VGE operation that results in a considerable improvement of the heat pumps cycle performance.

Table 4. Variable geometry ejector performance results and the required spindle and nozzle exit positions for different operating and ejector inlet conditions.

Op. conditions		Working fluid properties at ejector inlets					VGE performance		VGE control	
$T_{src_{in}}$	$\dot{Q}_{cond}$	$\dot{m}_p$	P_{ni}	T_{ni}	$\dot{m}_s$	P_{si}	CR_{VGE}	ER	SP	NXP
ºC	kW	g/s	bar	ºC	g/s	bar	-	-	mm	mm
70	20.1	77.4	12.1	120	43.7	2.0	1.30	0.565	5.3	13.8
75	22.4	86.2	12.1	120	50.4	2.3	1.26	0.585	6.2	12.0
80	24.9	95.6	12.1	121	57.8	2.7	1.23	0.605	7.2	10.5
85	27.5	106	12.1	121	66.1	3.1	1.20	0.625	8.5	9.2
90	30.3	117	12.1	122	75.2	3.5	1.17	0.646	10.2	8.1
95	33.3	128	12.1	123	85.3	4.0	1.14	0.667	12.5	7.1
100	36.5	140	12.1	123	96.4	4.5	1.12	0.688	16.9	6.3

Table 5. Characteristic ejector dimensions for the design operating conditions considering R601 working fluid (in mm unit).

d_{ni}	d_{nt}	d_{no}	d_{sc}	d_{mo}	d_d
10.9	3.45	6.90	40.0	12.4	46.7

The entrainment ratio and the achievable ejector compression ratio results are shown in Figure 8 for different heat pump temperature lift values. The compression ratios (P_8/P_7) in Table 4 and in Figure 8 represent the maximum value that guarantees double choked ejector operation. Looking at the results, one may note that for higher temperature lifts, the ejector can be operated with higher CR_{VGE} and lower entrainment ratio, which clearly indicates the increased benefit of applying ejectors in heat pump systems where relatively high temperatures lifts can be expected.

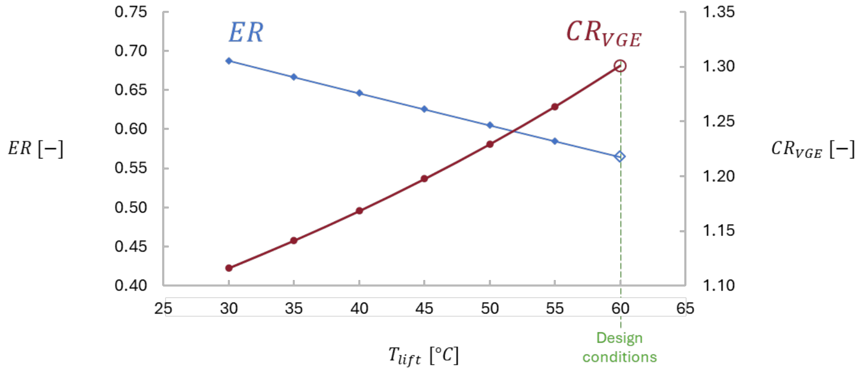

Figure 8. Entrainment ratio (ER) and achievable ejector compression ratio (CR_{VGE}) as a function of heat pump temperature lift T_{lift}.

5. Conclusions

The present work focused on the performance assessment and design of a high temperature heat pump cycle integrating a two-phase variable geometry ejector for expansion work recovery. The analysis was performed using a numerical model developed for the purpose based on simple formulations of the conservation laws. The variable geometry ejector model was developed on the constant pressure mixing ejector theory and on the assumption of homogeneous equilibrium of the phases. The model permitted the simulations for the heat pump cycle in two different configurations, with and without the integration of a variable geometry ejector, so that the benefit of the proposed system can be easily evaluated. Additionally, the model developed allowed for testing different low environmental impact working fluids for high temperature heat pump applications, with a heat output up to 130ºC. Based on the results presented, the following conclusions can be drawn:

- Among the five tested working fluids and for the considered operating condition range, R601 resulted in good cycle performance with relatively low compression ratios and compressor outlet temperatures. Additionally, using R601 leads to moderate condenser pressures;
- The application of a VGE reduces volume flow rate at mechanical compressor inlet and it varies significantly less with heat source temperature. This leads to both cost and operation stability benefits in comparison to a heat pump cycle using an internal heat exchanger only;
- Applying a VGE reduces the required mechanical compression ratio, which can extend compressor life time;
- The heat pump integrating a VGE outperformed the system integrating an IHX only with an average COP benefit of about 15%;
- The results indicated that the use of an ejector for partial expansion work recovery in a high temperature heat pump is especially beneficial for relatively high values of the temperature lift.

Nomenclature

Symbols

h	Fluid specific enthalpy	[J/ kg]
$\dot{P}_{mc}$	Compressor electric power	[kW]
$\dot{m}$	Mass flow rate	[kg/s]
$\dot{V}_{mc}$	compressor volumetric flow rate	[m^3/h]
$\dot{Q}_{cond}$	Heat pump heating capacity	[kW]
COP	Coefficient of performance	[-]
Ma	Mach number	[-]
v	Stream velocity	[m/s]
P	Fluid static pressure	[bar]
A	Cross section area	[m^2]
CR	Compression ratio	[-]
ER	Ejector entrainment ratio	[-]

Greek

ε	Heat exchanger efficiency	[-]
η	Efficiency constants	[-]
φ_{mix}	Ejector mixing efficiency	[-]
ϵ	Performance improvement	[%]
λ	Relaxation factor	[-]

Subscripts

c	Condenser
em	Electromechanical
mc	Mechanical compressor
vol	Volumetric
is	Isentropic
2f	Two-phase
d	Ejector diffuser
src	Source
e	Evaporator
in	Inlet
p	Primary
s	Secondary

Acknowledgements

The authors wish to acknowledge the financial support of “Fundação para a Ciência e a Tecnologia”, through contract PTDC/EME-TED/4043/2021. The authors would also like to express their gratitude to INEGI and FEUP institutions, for their support during the carried work. The authors wish to acknowledge the financial support of IS2H4C project, funded by the European Union under Grant Agreement No. 101138473.

References

[1] Abbasi MH, Abdullah B, Ahmad MW, Rostami A, Cullen J. Heat transition in the European building sector: Overview of the heat decarbonisation practices through heat pump technology. Sustainable Energy Technologies and Assessments 2021;48:101630. https://doi.org/10.1016/j.seta.2021.101630.

[2] Jesper M, Schlosser F, Pag F, Walmsley TG, Schmitt B, Vajen K. Large-scale heat pumps: Uptake and performance modelling of market-available devices. Renewable and Sustainable Energy Reviews 2021;137. https://doi.org/10.1016/j.rser.2020.110646.

[3] renewable energy agency I. Innovation landscape brief: Renewable power-to-heat. 2019.

[4] Bamigbetan O, Eikevik TM, Nekså P, Bantle M. Review of vapour compression heat pumps for high temperature heating using natural working fluids. International Journal of Refrigeration 2017;80:197–211. https://doi.org/10.1016/j.ijrefrig.2017.04.021.

[5] Marina A, Spoelstra S, Zondag HA, Wemmers AK. An estimation of the European industrial heat pump market potential. Renewable and Sustainable Energy Reviews 2021;139:110545. https://doi.org/10.1016/j.rser.2020.110545.

[6] Arpagaus C, Bless F, Uhlmann M, Schiffmann J, Bertsch SS. High temperature heat pumps: Market overview, state of the art, research status, refrigerants, and application potentials. Energy 2018;152:985–1010. https://doi.org/10.1016/j.energy.2018.03.166.

[7] Mateu-Royo C, Navarro-Esbrí J, Mota-Babiloni A, Barragán-Cervera Á. Theoretical performance evaluation of

ejector and economizer with parallel compression configurations in high temperature heat pumps. International Journal of Refrigeration 2020;119:356–65. https://doi.org/10.1016/j.ijrefrig.2020.07.016.
[8] Jiang J, Hu B, Wang RZ, Deng N, Cao F, Wang CC. A review and perspective on industry high-temperature heat pumps. Renewable and Sustainable Energy Reviews 2022;161. https://doi.org/10.1016/j.rser.2022.112106.
[9] Longo GA, Mancin S, Righetti G, Zilio C, Steven Brown J. Assessment of the low-GWP refrigerants R600a, R1234ze(Z) and R1233zd(E) for heat pump and organic Rankine cycle applications. Appl Therm Eng 2020;167:114804. https://doi.org/10.1016/j.applthermaleng.2019.114804.
[10] Arpagaus C, Bless F, Schiffmann J, Bertsch SS. Multi-temperature heat pumps: A literature review. International Journal of Refrigeration 2016;69:437–65. https://doi.org/10.1016/j.ijrefrig.2016.05.014.
[11] Bai T, Yan G, Yu J. Thermodynamic assessment of a condenser outlet split ejector-based high temperature heat pump cycle using various low GWP refrigerants. Energy 2019;179:850–62. https://doi.org/10.1016/j.energy.2019.04.191.
[12] Allouche Y, Bouden C, Varga S. A CFD analysis of the flow structure inside a steam ejector to identify the suitable experimental operating conditions for a solar-driven refrigeration system. International Journal of Refrigeration 2014;39:186–95. https://doi.org/10.1016/j.ijrefrig.2013.07.027.
[13] Tognoli M, Najafi B, Rinaldi F. Dynamic modelling and optimal sizing of industrial fire-tube boilers for various demand profiles. Appl Therm Eng 2018;132:341–51. https://doi.org/10.1016/j.applthermaleng.2017.12.082.
[14] Boccardi G, Botticella F, Lillo G, Mastrullo R, Mauro AW, Trinchieri R. Experimental investigation on the performance of a transcritical CO 2 heat pump with multi-ejector expansion system. International Journal of Refrigeration 2017;82:389–400. https://doi.org/10.1016/j.ijrefrig.2017.06.013.
[15] Varga S, Lebre PMS, Oliveira AC. CFD study of a variable area ratio ejector using R600a and R152a refrigerants. International Journal of Refrigeration 2013;36:157–65. https://doi.org/10.1016/j.ijrefrig.2012.10.016.
[16] Varga S, Oliveira AC, Palmero-Marrero A, Vrba J. Preliminary experimental results with a solar driven ejector air conditioner in Portugal. Renew Energy 2017;109:83–92. https://doi.org/10.1016/j.renene.2017.03.016.
[17] Pereira PR, Varga S, Soares J, Oliveira AC, Lopes AM, de Almeida FG, et al. Experimental results with a variable geometry ejector using R600a as working fluid. International Journal of Refrigeration 2014;46:77–85. https://doi.org/10.1016/j.ijrefrig.2014.06.016.
[18] Zhu Y, Huang Y, Li C, Zhang F, Jiang P-X. Experimental investigation on the performance of transcritical CO2 ejector–expansion heat pump water heater system. Energy Convers Manag 2018;167:147–55. https://doi.org/10.1016/j.enconman.2018.04.081.
[19] Gonçalves Jacinto K. ADVANCED NUMERICAL MODELLING OF COMPLEX SINGLE AND TWO-PHASE EJECTOR FLOWS. FACULDADE DE ENGENHARIA DA UNIVERSIDADE DO PORTO, 2025.
[20] Aidoun Z, Ameur K, Falsafioon M, Badache M. Current Advances in Ejector Modeling, Experimentation and Applications for Refrigeration and Heat Pumps. Part 2: Two-Phase Ejectors. Inventions 2019;4:16. https://doi.org/10.3390/inventions4010016.
[21] Ameur K, Aidoun Z, Falsafioon M. Experimental Performance of a Two-Phase Ejector: Nozzle Geometry and Subcooling Effects. Inventions 2020;5:23. https://doi.org/10.3390/inventions5020023.
[22] Kumar A, Yadav SK, Kumar V, Kulkarni A. A comprehensive exploration of ejector design, operational factors, performance metrics, and practical applications. Journal of the Brazilian Society of Mechanical Sciences and Engineering 2024;46:39. https://doi.org/10.1007/s40430-023-04618-8.
[23] Al-Doori G, Saleh K, Al-Manea A, Al-Rbaihat R, Altork Y, Alahmer A. A review of axial and radial ejectors: Geometric design, computational analysis, performance, and machine learning approaches. Appl Therm Eng 2025;266. https://doi.org/10.1016/j.applthermaleng.2025.125694.
[24] Wang L, Liu J, Zou T, Du J, Jia F. Auto-tuning ejector for refrigeration system. Energy 2018;161:536–43. https://doi.org/10.1016/j.energy.2018.07.110.
[25] Liu R, Zhu X, Wang X, Xiang R, Su L, Chu X, et al. Design and performance investigation on adjustable ejector with petal spindle valve for high-power fuel cell adapted heavy-duty truck powertrain. Appl Energy 2025;390. https://doi.org/10.1016/j.apenergy.2025.125774.
[26] Ameur K, Aidoun Z. A Simple Design Approach of Two-Phase Ejectors for CO2 Transcritical Heat Pumps. Journal of Applied Fluid Mechanics 2023;16:1887–900. https://doi.org/10.47176/jafm.16.10.1833.
[27] You C, Michel B, Revellin R. A novel 1-D single-mixed-flow homogeneous equilibrium model of two-phase ejector using CO2 as refrigerant. Energy 2025;322:135367. https://doi.org/10.1016/j.energy.2025.135367.
[28] Liu Y, Yu M, Yu J. An improved 1-D thermodynamic modeling of small two-phase ejector for performance prediction and design. Appl Therm Eng 2022;204:118006. https://doi.org/10.1016/j.applthermaleng.2021.118006.
[29] Huang BJ, Chang JM, Wang CP, Petrenko VA. A 1-D analysis of ejector performance. 1999.
[30] Flåtten T, Lund H. Equilibrium conditions and sound velocities in two-phase flows. 2010.
[31] Ameur K, Aidoun Z, Ouzzane M. Modeling and numerical approach for the design and operation of two-phase ejectors. Appl Therm Eng 2016;109:809–18. https://doi.org/10.1016/j.applthermaleng.2014.11.022.
[32] Giacomelli F, Mazzelli F, Banasiak K, Hafner A, Milazzo A. Experimental and computational analysis of a R744 flashing ejector. International Journal of Refrigeration 2019;107:326–43. https://doi.org/10.1016/j.ijrefrig.2019.08.007.
[33] Brennen CE. Fundamentals of Multiphase Flow. Cambridge University Press; 2005. https://doi.org/10.1017/CBO9780511807169.